A novel energy resolved X-ray computed tomography instrument for aviation security: Preliminary metrological investigation

Sloth, Steffen; Quagliotti, Danilo; De Chiffre, Leonardo; Christensen, Morten; Poulsen, Henning F.

Published in:
European Society for Precision Engineering and Nanotechnology, Conference Proceedings

Publication date:
2023

Document Version
Publisher's PDF, also known as Version of record

euspen's 23rd International Conference & Exhibition, Copenhagen, DK, June 2023
www.euspen.eu

A novel energy resolved X-ray computed tomography instrument for aviation security: Preliminary metrological investigation

Steffen Sloth[1,3], Danilo Quagliotti[2], Leonardo De Chiffre[2], Morten Christensen[3], Henning F. Poulsen[1]

[1]*Department of Physics, Technical University of Denmark, Fysikvej Building 307, 2800 Kongens Lyngby, Denmark*
[2]*Department of Civil and Mechanical Engineering, Technical University of Denmark, Koppels Allé Building 404, 2800 Kongens Lyngby, Denmark*
[3]*Exruptive A/S, Højnæsvej 75, 2610 Rødovre, Denmark*

Email address of the submitting author: stslot@dtu.dk

Abstract
The development of new high flux photon counting detectors (PCDs) opens the opportunity to implement energy dispersive x-ray computed tomography (XCT) systems in aviation security. This paper presents a novel prototype of an energy dispersive XCT instrument for research applications. The paper describes the instrument design and operational parameters along with a preliminary metrological investigation using a reference artefact, the CT tube, by visualisation and comparison to measurements on a coordinate measurement machine (CMM). The paper demonstrates how this novel CT instrument can, using only an extremely sparse number of 20 projections, both visualise the reference artefact with a 1 mm voxel size and be used to estimate distances with deviation from CMM around or less than half the voxel size (± 0.5 mm). This paper show that the novel prototype XCT instrument could be used to demonstrate the feasibility of a full-sized scanner design for future aviation security.

Keywords: CT visualisation, X-ray CT metrology, In-line X-ray CT, Aviation security.

1. Introduction

During the last decade, commercially available photon counting detectors (PCD) have evolved to operate with a sufficiently high flux to work in industrial applications [1-2]. This has led to several implementations of PCDs in medical scanners, where they offer a range of improvements. Utilising energy dispersive detection generally increases the amount of information that can be extracted from an acquisition [1-3].

Implementing PCDs in aviation security has in a research setting been shown to improve material classification capabilities [3-4]. Misclassification of passenger luggage is one of the main contributors to delays in an airport. Improving material classification can reduce the number of delays and provide a better experience for passengers. However, implementing PCDs in aviation security is not a trivial task, due to the limited spatial size of most available PCDs [1-2]. To cover a sufficiently large spatial range to scan passenger luggage multiple PCDs can be combined it a detector array. Industry partners have shown an interest in implementing such a detector array in a fixed-gantry in-line CT scanner design. An in-line scanner design comes with a series of challenges. A prototype instrument could help investigate the influence factor for the spectral response for material classification and geometry parameters for CT visualisation.

This paper presents a novel prototype of an energy dispersive XCT instrument and investigates some of the geometrical influence factors. The XCT instrument is presented in section 2, together with a reference artefact, the CT tube [5], used to study the performance of the instrument. Section 3 briefly discusses the state-of-the-art analysis pipeline developed for 3D CT reconstruction. The results of the study are shown and discussed in section 4. The conclusion in section 5 summarises the findings and reflects on future improvements and research needed to advance from a laboratory setting to operations in an airport.

2. Novel prototype energy dispersive x-ray CT instrument

Here the design and operation parameters of the energy dispersive x-ray CT instrument are explained. The instrument was originally designed for research testing of the PCD spectral response and not for geometric metrology. For this reason, it suffers from a series of inconveniences, as will be explained.

2.1. The x-ray CT instrument

A drawing of the instrument and its coordinate system is shown in figure 1.

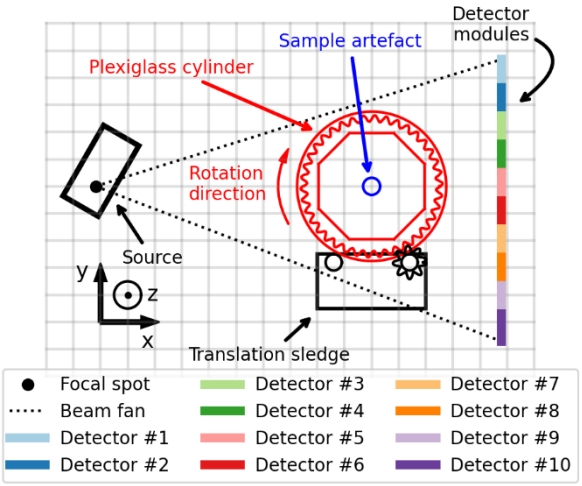

Figure 1. Illustration of the XCT instrument. The sledge translates along the z-axis (perpendicular to this 2D slice) and rotates clockwise. The legend indicates the detector numbering. The X-ray source is tilted by 30° around the z-axis.

The instrument can be broken into 5 parts. 1) the x-ray source emitting x-rays in a fan beam in the (x,y)-plane. 2) A linear array of ten 1D line PCDs with 128 pixels with a pixel size of 0.8x0.8 mm^2 and 128 energy channels. 3) An eight-sided cylinder of plexiglass. 4) A metal sledge for loading the plexiglass cylinder onto during an acquisition. 5) The reference artefact fixed via three clamps to a wooden base of the eight-sided plexiglass cylinder. The plexiglass cylinder, with the reference artefact fixed to its base, is loaded onto the sledge. During an acquisition the sledge is continuously translated with a linear motion past the line detector array, while a series of lines acquisitions are recorded. A full projection is captured after the sledge has passed by the detector array. Hereafter the sledges position is reverse back to its starting position. Between each projection the plexiglass cylinder, and thereby the reference artefact, is rotated clockwise around the direction of translation, as illustrated by the red arrow in the centre of figure 1. The control software allows for any number of projections and a combination of view angles. The instrument is designed to only required an extremely sparse number of projections for a CT reconstruction. For this study uses a total of 20 projections. This instrument serves as a prototype to demonstrate the feasibility of an in-line fixed-gantry energy dispersive x-ray CT scanner designed for aviation security, which has industrial interest due to the reduced acquisition time and improved threat detection capabilities [3-4].

The dimension of the projected images corresponds to the total number of pixels across all detectors in the vertical directions (here $10 * 128 = 1280$) and the number of acquired lines (N_{lines}) in the horizontal direction. The number of lines is determined by the set detector integration time ($t_{int.}$, minimum 5 ms), the acquisition length ($l_{acq.}$), and the linear translation speed of the sledge (v_{sledge}). The positive whole number value (rounded up) for the number of lines can be calculated by:

$$N_{lines} = \left\lceil \frac{|l_{acq.}|}{v_{sledge} * t_{int.}} \right\rceil \quad \textbf{(eq. 1)}$$

The denominator of eq. 1 defines the grid spacing along the translational direction (z-direction), which can be different from the grid spacing of the reconstructed 3D volume (x,y-directions).

Note that due to the linear stacking of the detector modules, a gap occurs between the last and first pixel on neighbouring detectors of around 0.5 mm.

Table 1. Overview of instrument parameters.

Component:	*Parameter*	*Value/type*
X-ray tube:	**Type**	**Spellman X5336**
	Target material	**Tungsten**
	Set current	**5 mA**
	Set voltage	**160 kV**
	Prefilters	**2 mm aluminium + 200 µm copper**
PCD detector:	**Type**	**DTX ME100 XC**
	Pixel size	**0.8 x 0.8 mm^2**
	Integration time	**5 ms**
	Binning mode	**Scanning mode**
	Energy channels	**128**
	Number of detector modules	**10**
	Gap between detector modules	**0.5 mm**
Translation system:	**Linear transverse translation speed**	**1) 20 mm/s 2) 160 mm/s**

An overview of the x-ray components and acquisition setting can be seen in Table 1. The instrument is placed in a temperature controlled and x-ray shielded room at the 3D Imaging Centre (3DIM) at the Technical University of Denmark (DTU). The temperature was monitored via a thermocouple placed near the sample to stay within (20.0 ± 1.0) °C during the acquisitions.

2.2. The reference artefact

The performance of this CT instrument with a resolution near 1 mm can be demonstrated by visualising a well-known artefact made of low x-ray absorbing materials such as the CT Tube [5] or the CT Crown [6]. However, due to the rotation being perpendicular to gravity, the CT Crown will be most resistant to bending: therefore, the CT tube is chosen as the reference artefact.

The CT tube is made of a carbon fibre tube of the type modulus Toray T700 oriented at 0° and 90°, which provides low x-ray absorption and high mechanical stability. The carbon fibre tube is 50 mm tall, has an outer diameter of around 63 mm, and has a wall thickness of 1.6 mm.

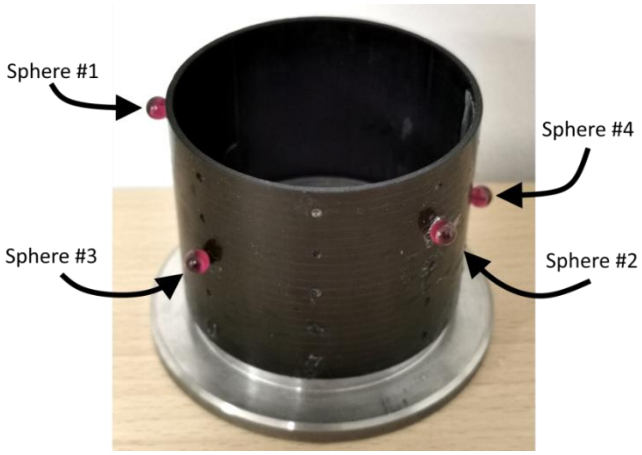

Figure 2. Picture of the CT tube reference artefact. The sphere numbering is used to define the sphere-to-sphere distances in table 2.

Four ruby spheres with a nominal diameter of 5 mm and a sphericity of 0.0006 mm have been trap-glued to the outer surface, see the picture in figure 2 The CT tube is placed on an invar plug for easier fixture in various instruments. The sphere's centre-to-centre distance has been measured on a coordinate measuring machine (CMM).

3. Data analysis

The data is reconstructed using specialised state-of-the-art reconstruction software. The reconstruction software uses a cone beam Algebraic Reconstruction Technique (ART) algorithm combined with Total-variation (TV) minimisation [7]. Iterative reconstruction techniques have been shown to improve the reconstruction quality of CT data with an extremely sparse number of projections [8]. To overcome the longer computation time of iterative algorithms the software utilises GPU parallelisation.

4. Results and discussion

This section shows and discusses the results acquired to study the instrument performance and demonstrate the performance via a 3D visualisation and a comparison of the sphere-to-sphere distances measured using this new CT instrument and a CMM.

4.1. 3D visualization of reference artefact

To study and demonstrate the performance of the x-ray CT instrument an acquisition of the CT tube has been reconstructed and is shown in figure 3. The acquisition was performed with the instrument parameters shown in table 1, and with a linear translational speed of 160 mm/s over 80 mm (100 lines). A total of 20 projections of the CT tube were acquired over an angular range of 300° with a sample rotation of 15° between each projection. The detector integration time was 5 ms per line, which set the total acquisition time per projection to 0.5 s.

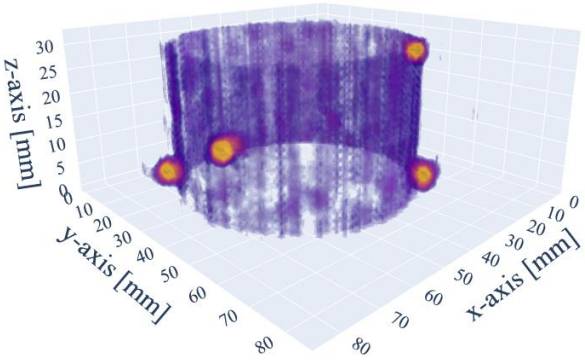

Figure 3. Visualisation of the reconstructed CT tube acquired using the CT scanner. The reconstruction used 20 image projections acquired with an angular stepping of 15°, a linear translation speed of 160 mm/s over 1000 lines, and the parameters in table 1. For each projection, all 128 energy channels are averaged together.

Using these acquisition parameters the grid spacing in the z-direction becomes 0.8 mm, which is equivalent to the pixel size. Initially, the energy dispersive data is rebinned into a single projection by averaging all 128 channels together. Each line was reconstructed independently into a 512x512 grid with a 1 mm grid spacing to mimic realistic conditions for an aviation security scanner. The 3D visualisation in figure 3 only shows the 80 slices containing the CT tube. The height axis (z-axis) has been rescaled by a factor of 0.8 mm to create a homogeneous voxel space.

The reconstructed volume in figure 3 shows a similar visual representation of the CT tube compared to the camera image in figure 2. The overall shape of the ruby spheres is spherical, but the shape can also be seen by the eye to have irregularities. This demonstrates the CT instrument's ability to visualise feature sizes on the millimetre scale.

4.2. Comparison with CMM measurements

To study the CT instrument's ability to perform length measurements, the sphere-to-sphere distances between the four ruby spheres are measured and compared with the distances measured using a Zeiss PRISMO CMM. The measurement uncertainty from the CMM is modelled by its maximum permissible error (MPE):

$$\mathrm{MPE}(\mathrm{E}_0)_{\mathrm{CMM}} = (0.90 + \mathrm{L}/350)\ \mu\mathrm{m}. \qquad \textbf{(Eq. 2)}$$

The uncertainty contribution from temperature fluctuations and the CMM measurements are found to be less than 0.1 µm and 5 µm, respectively, which is significantly smaller than the voxel size of 1 mm.

The CT data acquired for the comparison consist of three batches. In each batch five repeated measurements were acquired at two different linear translational speeds, giving two different grid spacings in the z-direction of 0.1 mm $(\mathrm{v}_{\mathrm{sledge}} = 20\ \mathrm{mm/s})$ and 0.8 mm $(\mathrm{v}_{\mathrm{sledge}} = 160\ \mathrm{mm/s})$. Similar to data for the visualisation in figure 3, have every acquisition a total of 20 projections each with 1000 lines and with 15° between projections. Table 1 lists the remaining instrument parameters. The CT instrument was shut down and the CT tube was removed from the fixture in between each batch to probe the reproducibility. The rotational orientation of the CT tube was changed between each batch. Table 2 list the six measurands of the sphere-to-sphere distances.

From a 3D reconstructed volume, the sphere-to-sphere distances are measured by the distance between the sphere's centre position estimated from a least-square fit of a sphere's boundary voxels.

Table 2. Overview of the six measurands for the distances between the four ruby spheres numbered in figure 2.

Measurand	*Start sphere*	*End sphere*
D1	Sphere #1	Sphere #2
D2	Sphere #1	Sphere #3
D3	Sphere #1	Sphere #4
D4	Sphere #2	Sphere #3
D5	Sphere #2	Sphere #4
D6	Sphere #3	Sphere #4

The deviation of the measurands in table 2 measured using the CT instrument from the CMM measurement are shown in figures 4 and 5 for a z-spacing of 0.8 mm and 0.1 mm, respectively.

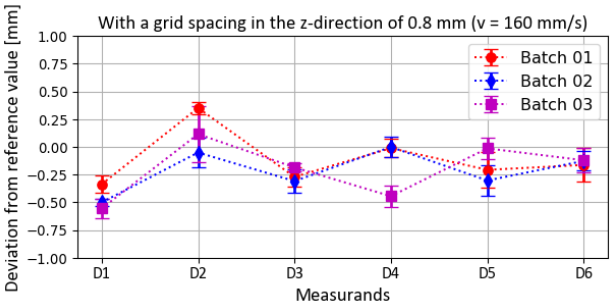

Figure 4. Mean deviation of each of the three batches of CT measurements from the CMM measurements of the six measurands. The sledge in the CT instrument was translated with 160 mm/s. resulting in a grid spacing of 0.8 mm in the z-direction. The error bars are evaluated as two times the standard deviation of the five repeated measurements (confidence level of around 95%).

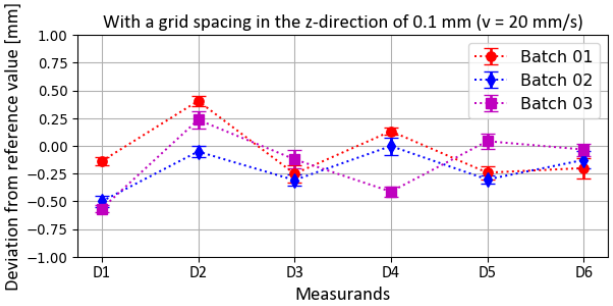

Figure 5. Mean deviation of each of the three batches of CT measurements from the CMM measurements of the six measurands. The sledge in the CT instrument was translated with 20 mm/s. resulting in a grid spacing of 0.1 mm in the z-direction. The error bars are evaluated as two times the standard deviation of the five repeated measurements (confidence level of around 95%).

The error bars in figures 4 and 5 are calculated from two times the standard deviation of the five repeated measurements in each batch. The deviations from the CMM measurement are within ± 0.5 mm which is half the voxel size. This demonstrates

the new CT instrument can be used to evaluate different lengths in the range from around 30 mm to 60 mm with a 1 mm voxel size at different translational speeds.

A similar trend is observed between the measurements of different translational speeds, where the deviation of, e.g., batch 3 in figure 4 is similar to the same batch in figure 5 (where the CT tube has the same orientation). This indicates that the deviation of the sphere-to-sphere distance is related to the sphere's position. It is suspected that the deviation is associated with the angular sampling of the ruby sphere, which is only acquired over a range of 300°. This is not investigated further, since the effect is smaller than the voxel size.

The sphere-to-sphere distances should be the same across batches and averaging them indicates the CT instruments' reproducibility, as seen in figure 6.

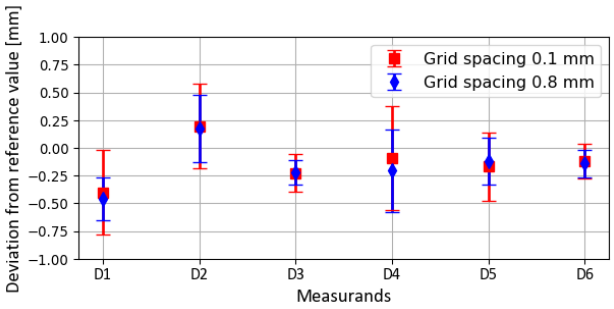

Figure 6. Deviation of the 3 batches averaged together from the CMM measurements of the six measurands. The two data series are acquired using different linear translation speeds of the sledge, resulting in different grid spacing along the z-direction (translational direction) of the reconstructed volumes. The error bars are evaluated as two times the standard deviation (confidence level of around 95%) of fifteen repeated measurements (combination of all three batches).

Comparing the error bars of figures 4 and 5 to those of figure 6 illustrates the significant differences between the repeatability and reproducibility that can be achieved for length measurement using the new CT instrument. The error bars in figure 6 are two times the standard deviation of the fifteen repeated measurement (combining the three batches) of each measurand. All mean values are near or less than ± 0.5 mm of the reference values measured on the CMM and the absolute values of two times the standard deviation is all less than ± 0.5 mm for all measurands. This demonstrate the instruments reproducibility is within the grid spacing of the reconstruction volume for length measurement in 30 mm to 60 mm range.

5. Conclusion and outlook

This paper describes a novel in-line x-ray CT instrument designed to mimic a fixed-gantry in-line x-ray CT scanner for aviation security. The new instrument uses PCD which offers the ability to improve the material classification of items within passenger luggage. Here the geometrical capability was investigated in a preliminary studied and demonstrated by repeated acquisition of a reference artefact, the CT tube. A 3D visualisation of the CT tube was reconstructed from 20 acquired projections and shown in figure 3 with a 1 mm volume grid spacing. This illustrates that such a CT instrument design can yield visualisations of artefacts with millimetre sized features. Repeated measurements of the sphere-to-sphere distance of the four ruby spheres were compared to CMM measurements. The comparison showed a good agreement of the distances measured on the two instruments with a deviation around or less than half the voxel size (± 0.5 mm). Estimating the reproducibility of the CT measurements yields a standard deviation less than the full voxel size (< 1.0 mm). These results indicate the ability to compare distances on the scale of 30 mm to 65 mm with a deviation less than the voxel size from measurements using the new CT instrument.

Before such a system can be upscaled and tested in an aviation security environment further insight into the instrument behaviour is required. We find that the most important task is a thorough metrological investigation of the instrument. This investigation would include measurements of different reference artefacts with length scales more alike to passenger luggage and measurements of the scanner's structural resolution. Future research would be helped by constructing a new prototype version of the instrument with the axis of translation being parallel to gravity. This would greatly ease the challenges of sample fixture and remove the undesired bias from gravity while still relating to a fixed-gantry in-line instrument design with industrial interest.

Acknowledgements

This work was performed at the Danish National Facility for Imaging with X-rays (DANFIX) and supported by the Innovation Fund Denmark (grant ref. number 1044-00087B) and the company Exruptive A/S. The authors would like to thank Klaus Liltorp for helpful discussions and assistance with CMM measurements.

References

[1] Ren L, Zheng B, Liu H. Tutorial on X-ray photon counting detector characterization. Journal of X-ray science and technology. 2018 Jan 1;**26**(1): pp 1-28.

[2] Flohr T, Petersilka M, Henning A, Ulzheimer S, Ferda J, Schmidt B. Photon-counting CT review. Physica Medica. 2020 Nov 1;**79**: pp 126-36.

[3] Busi M, Kehres J, Khalil M, Olsen UL. Effective atomic number and electron density determination using spectral x-ray CT. InAnomaly Detection and Imaging with X-rays (ADIX) IV 2019 May 14 (**Vol. 10999,** pp. 7-17). SPIE.

[4] Jumanazarov D, Koo J, Poulsen HF, Olsen UL, Iovea M. Significance of the spectral correction of photon counting detector response in material classification from spectral x-ray CT. Journal of Medical Imaging. 2022 Jun; **9**(3):034504.

[5] Stolfi A and De Chiffre. L (2016). 3D artefact for concurrent scale calibration in Computed Tomography. Annals of the CIRP, **65**(1), pp. 499-502. DOI: 10.1016/j.cirp.2016.04.069.

[6] Stolfi A and De Chiffre. L (2016). CT crown for on-machine scale calibration in Computed Tomography. In Proceedings of the 16th International Conference of the European Society for Precision Engineering and Nanotechnology, Nottingham, United Kingdom, P1.34. ISSN 978-0-9566790-8-6.

[7] Sidky E Y and Pan X., Image reconstruction in circular cone-beam computed tomography by constrained, total-variation minimization. Physics in Medicine & Biology, 53(17) (2008), p.4777.

[8] Sidky EY, Kao CM, Pan X. Accurate image reconstruction from few-views and limited-angle data in divergent-beam CT. Journal of X-ray Science and Technology. 2006 Jan 1;**14**(2):119-39.